X-ray-absorption studies of electron doping and band shifts in $R_{2-x}Ce_xCuO_{4-\delta}$ (R =Pr, Nd, Sm, Eu, and Gd)

G. Liang, Y. Guo, D. Badresingh, and W. Xu
Department of Physics, Sam Houston State University, Huntsville, Texas 77341

Yijie Tang
Department of Chemistry, Sam Houston State University, Huntsville, Texas 77341

M. Croft, J. Chen, and A. Sahiner
Department of Physics, Rutgers University, Piscataway, New Jersey 08855

Beom-hoan O and J. T. Markert
Department of Physics, University of Texas, Austin, Texas 78712
(Received 27 September 1993; revised manuscript received 15 September 1994)

We have measured the polarized x-ray-absorption spectra at the Cu K edge of $Nd_{2-x}Ce_xCuO_{4-\delta}$ single crystals and the unpolarized spectra of $R_{2-x}Ce_xCuO_{4-\delta}$ (R =Pr, Nd, Sm, Eu, and Gd) ceramic samples. The results indicate that up to the T'-phase stability limit (and including the narrow region of superconductivity), Ce doping continuously donates electrons into the Cu 3d orbitals. Our results evidence a Cu^{1+} content in these T'-phase materials which increases almost linearly with the Ce-doping level x, and an electron doping fraction from each Ce atom to Cu which is quite close to unity (except in the R=Gd series). It is found that the size variation of the rare-earth elements R causes a number of feature changes in the Cu K edge, including an about 0.5 eV upward edge shift. These effects are explained by the ligand field shift of the unoccupied Cu 4p and 3d bands. A cluster model description has been developed to correlate the spectral features of the Cu K-edge spectra to different 3d configurations. The experimental results can be well described by the following model parameters: Cu 1s-3d Coulomb interaction $U_{cd}\sim 6.5$ eV, Cu 1s-O 2p Coulomb interaction $U_{cL}\sim 1.1$ eV, d-ligand hybridization $V\sim 2.7$ eV, Cu↔O charge-transfer energy $\Delta\sim 1.3$ eV (at $x=0$), and $\Delta\sim 0.5$ eV (at $x=0.2$).

I. INTRODUCTION

In spite of extensive spectroscopic studies, the nature of the charge carriers and the electronic structure in the n-type oxide superconductors $R_{2-x}A_xCuO_{4-\delta}$ (R =rare-earth elements and A =Ce, Th) (Refs. 1–3) are still not fully understood. While all the Ce L_3 x-ray absorption spectra[4–7] (XAS) and Ce 3d emission results clearly support electron doping, the Cu 1s, 2p, and O 1s XAS,[4–7,11–15] x-ray photoemission spectroscopy (XPS),[6,8–10,16–19] and electron-energy-loss spectroscopy[20–22] (EELS) results have led to conflicting conclusions regarding whether the electrons are doped from Ce into localized Cu 3d orbitals or other extended bands. In particular uncertainties in the interpretation of the XAS Cu K-edge results could be due partially to the lack of the polarized data on doped single crystals, from which the spectral features and their modifications can be unambiguously identified.

In this paper we will discuss two groups of experimental Cu K-edge studies on these materials. In the first the polarized edge spectra for the R =Nd system will be analyzed within a cluster model. In the second the electronic structure modifications induced by varying R across the rare-earth series will be discussed.

The polarized Cu K-edge results reported by Tan *et al.*[22] on the $Pr_{2-x}Ce_xCuO_4$ is particularly interesting. They interpreted their results in terms of a Ce doping induced almost rigid shift in the $E\perp c$ spectra and production of a new d^{10} feature in the $\mathbf{E}\|c$ spectra. Thus, they proposed that the upper unoccupied band, consisting of predominantly Cu 3d states, shifts downwards, and concluded that Ce doping injects electrons from Ce atoms into the localized Cu 3d orbital. This work provided a new understanding of the electron doping mechanism and clarified the interpretation of the Cu K-edge XAS data of polycrystalline $Nd_{2-x}Ce_xCuO_4$.[4–7,11–13] However, since the XAS results of Tan *et al.* were only reported for compounds with $0\le x\le 0.12$, the proposed electron doping and in the high-level Ce-doping region (where the superconducting transition occurs), are not yet clear. Thus, a polarization Cu K-edge study extended to the high-level Ce-doped ($x>0.12$) compounds is needed.

In the present study, we report the polarized Cu K-edge XAS results on high-level Ce-doped $Nd_{2-x}Ce_xCuO_4$ single crystals. It should be noted that even though the $Nd_{2-x}Ce_xCuO_4$ system is the most widely studied n-type superconductor system, there is so far no report on the polarized Cu K-edge data for the doped compounds[4–7,11–13] in this series. The results presented here for the high-level Ce-doped crystals provide a test of the electron-doping mechanisms proposed

by Tan *et al.*[22] Furthermore, with the combination of the polarized Cu K-edge data in both the low- and high-x region, a cluster model is proposed to interpret the spectral features. The justification of extending the use of the cluster model from XPS to Cu K-edge XAS was recently discussed by Tolentino *et al.*[23] In the present work, we use the cluster model to analyze the Cu K-edge XAS data for doped n-type superconductors and give a rough estimate of the cluster model parameters.

We also present systematic Cu K-edge spectra for $R_{2-x}Ce_xCuO_{4-\delta}$ with R including all of the rare-earth elements (Pr, Nd, Sm, Eu, and Gd) (Refs. 1–3,24) which stabilize the T' phase.[25,26] It has been found that, in contrast with the p-type 1:2:3 superconductors in which T_c is almost unchanged with R-element variation,[27–29] the T_c in these n-type superconductors are strongly R-element dependent[1–3,30] even though all of the R elements are trivalent.[21,31] The mechanism for such a dependence is still unclear. It is possible that this dependence is related to the changes in electronic structure of the CuO_2 layer induced by R-element variation. For example, Tan *et al.* have suggested that the shift of the unoccupied Cu bands in $Pr_{2-x}Ce_xCuO_4$ (Ref. 22) may be related to the a lattice parameter expansion, thus, it is expected that such a band shift should also occur when the R elements vary from larger size to smaller size. We intend to provide the electronic structure information related to the variation of rare-earth elements.

II. EXPERIMENT

The single crystals of $Nd_{2-x}Ce_xCuO_{4-\delta}$ with $x=0.15$ and 0.20 were grown from CuO-rich composition of the high-purity starting materials Nd_2O_3 (99.99%), CeO_2 (99.99%), and CuO (99.999%). Approximately 40 g of predried starting materials with overall composition $Nd_{1.73}Ce_{0.27}Cu_{4.7}O_y$ and $Nd_{1.77}Ce_{0.23}Cu_{4.7}O_y$ for the $x=0.20$ and 0.15 samples, respectively, were mixed and fired in air several times at $\approx$1000 °C in 50-ml alumina crucible. The mixtures were then heated to 1240 °C for 1 h and cooled at a rate of 5 °C/h to 940 °C, and removed to air. Many mm-size crystals were mechanically removed from cavities in the flux. The Ce contents were determined from energy dispersive spectroscopy (EDS) and electron microprobe (wavelength dispersive spectroscopy, WDS), with a series of ceramic calibration standards, and are accurate to $\Delta x=\pm 0.02$. The $x=0.20$ crystal was annealed in oxygen at 950 ° C and cooled slowly to room temperature. The $x=0.15$ sample was reduced at 890 °C in flowing He gas for 16 h, and quenched to room temperature. This crystal displayed diamagnetism at 10 K in dc SQUID measurements in a 10-Oe field. The preparation and characterization of the undoped $x=0.00$ single crystal have been described elsewhere by Tan *et al.*[22]

The polycrystalline samples of $R_{2-x}Ce_xCuO_{4-\delta}$ were prepared by solid-state reaction from predried starting materials, with several firings at 900 and 1000 °C (about 1 week total with intermediate grindings), then pressed into large pellets. The pellets were then fired at 1080 °C for 2 days, and then fired in flowing oxygen at 950 °C and slow-cooled to room temperature at 25 °C/h. The pellets were then cut in half, the reduced samples were made by annealing the second half of each pellet in flowing He at temperatures ranging from about 800 to 900 °C for about 16 h, then rapidly cooled to room temperature. Thermogravimetric analysis was used to identify the temperature at which oxygen loss begins to occur for selected specimens; along with past experience and past iodometric titrations, we chose temperatures which we believe correspond to $\delta=0.02$, and indeed the measured values of δ are 0.0 within the experimental error of ± 0.02. In general, we find that the larger the rare-earth host ion, or the greater the Ce concentration, the higher the reduction annealing temperature required for a given oxygen loss. The T' phase of the samples was confirmed by x-ray-diffraction measurements. The oxygen deficiency δ in the oxygen reacted samples was determined by titration to be $\delta=0.00$.

The x-ray-absorption measurements were carried out at the National Synchrotron Light Source on beam line X-11A using a Si(111) monochromator and 0.5-mm entrance slit. The spectra for single crystals were measured using fluorescence detection mode while the unpolarized spectra for powder polycrystalline samples were obtained using transmission detection mode. The degree of linear polarization as a percentage of total is about 99.6% at the energy of the Cu K edge ($\sim$9 keV). To obtain higher signals for the single crystals, collages of similarly oriented small crystals (each about $3\times3\times0.1$ mm) were carefully assembled on scotch tape. Energy calibration was made by simultaneously measuring the absorption spectra of a Cu metal or a Cu_2O powder reference. For convenience of discussion, we have chosen the energy of the preedge peak in the spectrum of Cu_2O as the zero energy. All of the spectra presented in this paper have been background subtracted and normalized in the same energy region.

III. Cu K-EDGE XAS-3d CONFIGURATION CORRELATION: A CLUSTER MODEL DESCRIPTION

Attempts to understand high-T_c superconductivity have involved models related to Anderson lattice and multiple-band Hubbard models.[32–34] A simple local cluster model[35] incorporating both 3d correlation and 3d-2p hybridization effects has been successfully used to interpret the features of the XPS spectra (such as Cu 2p spectra) (Refs. 8,17,35–37) of Cu oxides and both p- and n-type cuprate high-T_c superconductors (HTS). The extension of using a cluster model from XPS to XAS (e.g., Cu K edge) for some cuprate insulators has been recently discussed by Tolentino *et al.*[23] We will follow the spirit of Tolentino's discussion; however, the emphasis will be focused on the interpretation of the new Cu d^{10} feature occurring in the Cu K edge of the n-type superconductors $R_{2-x}Ce_xCuO_{4-\delta}$.

Cu compounds such as CuO or undoped cuprates such as Nd_2CuO_4 are usually well described as charge-transfer-type insulators.[37] In the Cu K-edge absorption process of these insulators, the initial states (the states before absorbing a photon) of Cu including the Cu 3d–O 2p hybridization can be described as linear combinations of

$3d^9$ and $3d^{10}\underline{L}$ configurations, where $\underline{L}$ denotes a hole in the ligand O $2p$ states. During the absorption, a Cu $1s$ core hole is produced, thus, the final (or core-hole) states reached in XAS should be described as linear combinations of $\underline{c}d^9 4p$ and $\underline{c}d^{10}\underline{L}4p$ configurations, where $\underline{c}$ represents the Cu $1s$ core hole. If the hybridization matrix element is represented by V then a simple matrix calculation similar to that of Shen *et al.*[35] would lead to the energy diagram shown on the left part of Fig. 1. Here Δ is the energy separation between the two configurations of the initial states. The final-state energy separation is $\Delta' = U_{\underline{c}d} - U_{\underline{c}\underline{L}} - \Delta$, with $U_{\underline{c}d}(U_{\underline{c}\underline{L}})$ representing the Coulomb interaction between the Cu $1s$ hole and the Cu $3d$ (O $2p$) hole. One should note that the $U_{\underline{c}\underline{L}}$ introduced here is a new parameter which has not been previously used in models for the interpretation of spectroscopic data. We believe that the necessity of introducing this parameter in the model is similar to the necessity of introducing the Coulomb interaction (~ 1.2 eV) between the O $1s$ hole and Cu $3d$ hole in the interpretation of O K-edge spectra of the p-type superconductor $La_{2-x}Sr_xCuO_{4+\delta}$.[38]

Within this two-level model, the ground and excited states of the initial states can be expressed as

$$|\Psi_{\text{g.s.}}\rangle = \cos\theta |d^9\rangle - \sin\theta |d^{10}\underline{L}\rangle , \quad (1)$$

$$|\Psi_{\text{ex}}\rangle = \sin\theta |d^9\rangle + \cos\theta |d^{10}\underline{L}\rangle , \quad (2)$$

with $\tan(2\theta) = 2V/\Delta$. Similarly, the two final states are

$$|\Psi_{\text{fin},1}\rangle = -\sin\theta' |\underline{c}d^9 4p\rangle + \cos\theta' |\underline{c}d^{10}\underline{L}4p\rangle , \quad (3)$$

$$|\Psi_{\text{fin},2}\rangle = \cos\theta' |\underline{c}d^9 4p\rangle + \sin\theta' |\underline{c}d^{10}\underline{L}4p\rangle , \quad (4)$$

with $\tan(2\theta') = 2V/(U_{\underline{c}d} - U_{\underline{c}\underline{L}} - \Delta)$. The transitions of the ground state into the final states $|\Psi_{\text{fin},1}\rangle$ and $|\Psi_{\text{fin},2}\rangle$ yield a K edge which is a superposition of two edge features separated by an energy of

$$\delta E_1 = \sqrt{(U_{\underline{c}d} - U_{\underline{c}\underline{L}} - \Delta)^2 + 4V^2} . \quad (5)$$

If $U_{\underline{c}d}$ is much larger than the other parameters, then the mixing of $|\underline{c}d^9 4p\rangle$ in $|\Psi_{\text{fin},1}\rangle$ and $|\underline{c}d^{10}\underline{L}4p\rangle$ in $|\Psi_{\text{fin},2}\rangle$ (i.e., $|\sin\theta'|^2$) can be quite small. In such a case, the intensities of these two features (e.g., the Cu K-edge double features A and B or C and D in Fig. 2) are approximately related to the weight of each configuration ($|d^{10}\underline{L}\rangle$ and $|d^9\rangle$) in the ground state. The intensity ratio of the double features is approximately

$$I_{\text{rel}} = I_C/I_D = \alpha(\langle\Psi_{\text{g.s.}}|\Psi_{\text{fin},1}\rangle/\langle\Psi_{\text{g.s.}}|\Psi_{\text{fin},2}\rangle)^2 = \alpha\tan^2(\theta+\theta') , \quad (6)$$

where α is a constant.

Next, we discuss the effects of Ce doping on the predominantly $d^9 - d^{10}\underline{L}$ ground state of Cu in Nd_2CuO_4. The Ce doping could inject extra electrons into either the $3d$ orbitals of the Cu sites with d^9 state or the $2p$ orbitals of the ligand O sites associated with the $d^{10}\underline{L}$ state. In both of these two cases, the d^{10} state of Cu is formed (via $d^9 + e^- \rightarrow d^{10}$ and $d^{10}\underline{L} + e^- \rightarrow d^{10}$ processes, respectively) without involving the energy U required in the Hubbard model. The electrostatic potential argument, as

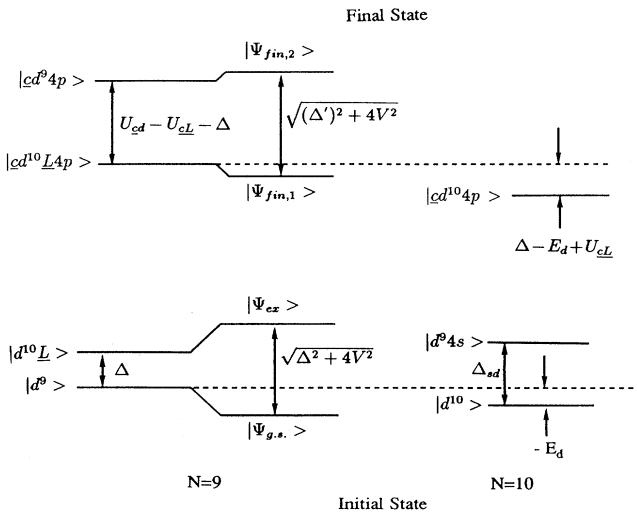

FIG. 1. Energy-level diagram for configurations of the cluster model description of the initial and final states for Cu K XAS. N is the number of d electrons of the pure d configuration (without hybridization effects) in the cluster model. $N = 10$ corresponds to the injection of an electron from Ce into a Cu orbital.

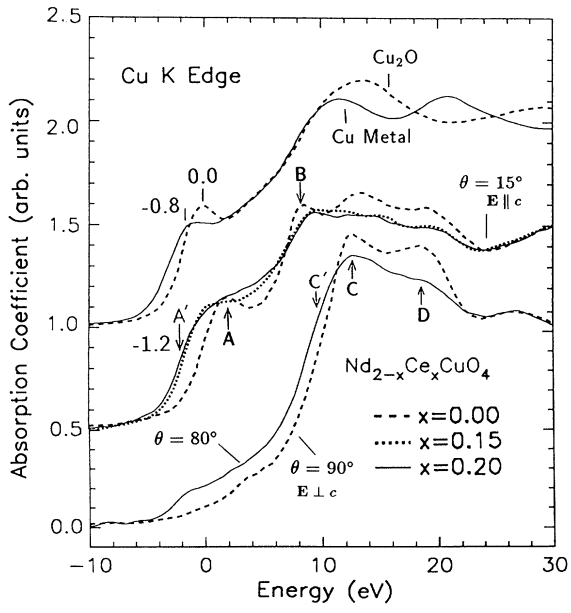

FIG. 2. Polarized Cu K-edge spectra for single crystals $Nd_{2-x}Ce_xCuO_{4-\delta}$ with $x = 0$ (dashed curve), 0.15 (dotted curves), and 0.2 (solid curves). θ is the angle between the **E** vector and the c axis of the crystal. The spectra of polycrystalline Cu metal and Cu_2O are also shown for reference. The final states (and final d orbital configurations) associated with the feature assignments in the figure are A', $4p_\pi(d^{10})$; A, $4p_\pi(d^{10}\underline{L})$; B, $4p_\pi(d^9)$; C', $4p_\sigma(d^{10})$; C, $4p_\sigma(d^{10}\underline{L})$; and D, $4p_\sigma(d^9)$. Note that the intensities of the d^{10} features A' and C' increase with Ce doping while the intensities of the other features A through D decrease.

pointed out by Tranquada *et al.*,[4] favors the former electron-doping process over the latter and this is indeed supported by the O K-edge results.[14,20] The fraction of electrons doped into the Cu 4s orbitals should be negligible small because the local Cu 3d to 4s excitation energy ($\sim$4–5 eV) (Ref. 38) is usually quite large and these orbitals are neglected. Neglecting higher-lying states, intersite hopping only redistributes the d^{10} sites without altering their population. Thus the d^{10} state population should be proportional to the Ce concentration x and to the fractional efficiency of Ce doping into the planes.

The energy level of Cu d^{10} is shown in the right part of Fig. 1, where $-E_d$ is the binding energy [with typical value of 2.0 eV (Ref. 35) obtained from XPS data on p-type cuprate superconductors] of an electron added to the 3d hole. The initial and final (core hole) $3d^{10}$ states are denoted in Fig. 1 by $|d^{10}\rangle$ and $|\underline{c}d^{10}4p\rangle$, respectively. We will interpret the A' and C' features (the d^{10} features) in the polarized spectra of the Ce-doped samples (see Fig. 2) as corresponding to the transition of Cu from $|d^{10}\rangle$ to $|\underline{c}d^{10}4p\rangle$. The energy difference between the energy required for this transition and that required for the transitions from $|\Psi_{\text{g.s.}}\rangle$ to $|\Psi_{\text{fin},1}\rangle$ (mainly $|d^{10}\underline{L}\rangle$) is

$$\delta E_2=\tfrac{1}{2}(\sqrt{\Delta^2+4V^2}+\Delta)-\tfrac{1}{2}(\sqrt{\Delta'^2+4V^2}-\Delta')+U_{c\underline{L}}\ , \tag{7}$$

which should correspond to the energy separation between the feature A' and A in Fig.2 .

IV. POLARIZED SPECTRA OF $Nd_{2-x}Ce_xCuO_{4-\delta}$ SINGLE CRYSTALS

A. Polarized Cu K-edge spectra: Feature identification

In Fig. 2, we compare the polarized Cu K-edge spectra of the doped crystals ($x=0.15$ and 0.2) with those of the undoped sample ($x=0.0$). It is clear from the single-crystal data that features A and B are only present in the $\mathbf{E}\|c$-axis (or $\theta=15°$) spectrum while feature C and D are most prominent in the $\mathbf{E}\perp c$-axis (or $\theta=90°$) spectrum. The small components of the C and D features visible in the $\theta=15°$ spectrum could be due to the small in-plane component of x-ray polarization vector $\mathbf{E}$. These double-peak features can be interpreted in a similar way to those previously used for the undoped Nd_2CuO_4 crystal,[12,22] i.e., the features A and B in the $\mathbf{E}\|c$ spectrum are assigned to the 1s to out-of-plane $4p_\pi$ states transitions, whereas the features C and D in the $\mathbf{E}\perp c$ spectrum are due to the transitions from 1s to the in-plane $4p_\sigma$ states. The lower-energy A and C features involve "shakedown" final states in which the core hole is better screened (relative to the B and D related processes) by ligand to metal charge transfer.[39,40] These final states are usually denoted by $3d^{10}\underline{L}$, where $\underline{L}$ denotes a hole on the ligand shell.

Tan *et al.*[22] first identified the A' feature as due to $1s\rightarrow 4p_\pi$ transition with Cu in a $3d^{10}$ configuration in their XANES study on single-crystal $Pr_{2-x}Ce_xCuO_{4-\delta}$ with $0\le x\le 0.12$. This identification was made based on the fact that the A' feature can be observed only in the $\mathbf{E}\|c$ Cu K-edge spectra of the Ce-doped crystals and that the energy position of the feature is close to but below the positions of the $4p_\pi$ features of Cu_2O and Cu metal. Our polarized Cu XANES data on the heavily Ce-doped $Nd_{2-x}Ce_xCuO_{4-\delta}$ with $x\ge 0.15$ support this assignment for feature A'. The very weak intensity of A' feature visible in the $\mathbf{E}\perp c$ ($\theta\approx 80°$) spectrum of the $x=0.2$ sample can be attributed to the small out-of-plane component of $\mathbf{E}$. The value of θ was set to be about 80° for the $x=0.2$ sample (rather than 90° as for the undoped sample) to avoid the Bragg reflection features in the near-edge region. The absence of the A' feature in the spectra of the undoped sample indicates that A' feature is associated with Ce doping. On the other hand, the absence of the A' feature in the $\mathbf{E}\perp c$ spectra of our high-level doped $Nd_{2-x}Ce_xCuO_{4-\delta}$ suggests that this feature is $4p_\pi$ state related. The locations of the feature A', as determined by the peak positions of the difference spectrum (obtained by subtracting the spectra of $x=0.0$ sample from that of the $x\ge 0.15$ samples) are 3.2 eV below the well-screened $4p_\pi$ feature A of the $x=0.0$ sample. This value is exactly the same as that reported for the low-level ($x\le 0.12$) Ce-doped $Pr_{2-x}Ce_xCuO_{4-\delta}$ crystals.[22]

Comparing the C peaks of the $\mathbf{E}\perp c$ spectra of the $x=0.0$ and 0.2 materials (in Fig. 2), we note that the $x=0.2$ C feature is broadened on the low-energy side. Two contributions could contribute to this effect: a downward edge shift as proposed by Tan *et al.* and discussed later in this paper; and the appearance of a new C' feature 3.2–3.5 eV below the C-feature peak located at $\sim$12.7 eV. Such a C' feature would be the in-plane analogy of the A' feature with the identification $1s\rightarrow 4p_\sigma$ with a Cu $3d^{10}$ configuration. The Ce-doping induced intensity increase of the A' and C' features, accompanied by the simultaneous intensity decrease of the unprimed features A, B, C, and D (as discussed in next section), does modify the shape of the $\mathbf{E}\|c$ and $\mathbf{E}\perp c$ edges to some degree. Further consideration of the potential relative roles of the C' feature and the edge shift will be made in the context of the rest of our results (particularly those on the compression induced edge-shift) in the discussion section (Sec. V D), where the C' feature interpretation will be shown to be more satisfactory relative to the edge-shift interpretation.

By comparing the energy level scheme in Fig. 1 and the relative positions of the features in Fig. 2, one can make the following assignments in terms of cluster model: A (as well as C) and B (as well as D) correspond, respectively, to the transitions of Cu from $|\Psi_{\text{g.s.}}\rangle$ into the final states $|\Psi_{\text{fin},1}\rangle$ and $|\Psi_{\text{fin},2}\rangle$, but for features A and B the photoelectron is in the Cu $4p_\pi$ state while for features C and D the photoelectron is in the Cu $4p_\sigma$ state. Feature A' (and C') is due to transition from the initial state $|d^{10}\rangle$ into final state $|\underline{c}d^{10}4p\rangle$ with the photoelectron in a Cu $4p_\pi$ (and $4p_\sigma$) orbital. With these identifications, the experimental values for δE_1 in Eq. (5) and δE_2 in Eq. (7) should be roughly the observed 6.7 ± 0.3 eV energy separation between features A and B (or C and D) for the undoped crystal and the 3.2-eV energy separation between features A' and A for the doped crystal, respectively. For $Nd_{2-x}CuO_{4-\delta}$, the values of Δ and V deduced from

Cu $2p$ XPS data range from 1.0 to 1.55 eV and from 2.5 to 3.0 eV, respectively. The value of Δ deduced from recent optical reflectivity and Raman-scattering data is about 1.45 eV.[41] If we use 1.35 eV for Δ and 2.7 eV for V, then the values obtained from solving Eqs. (5) and (7) are 6.5 ± 0.4 eV for $U_{\underline{c}d}$ and 1.1 ± 0.1 eV for $U_{\underline{c}\underline{L}}$. The 6.5 eV $U_{\underline{c}d}$ indicates that the Cu $1s$-$3d$ hole Coulomb interaction is comparable to the Cu $2p$-$3d$ hole Coulomb interaction, which is ~5.5 eV, as deduced from Cu $2p_{3/2}$ soft-x-ray -absorption spectra.[15] The 1.1 eV $U_{\underline{c}\underline{L}}$ between the Cu $1s$ and O $2p$ holes, however, is quite close to the ~1.2-eV Coulomb interaction between the O $1s$ and Cu $3d$ holes.[38] With these model parameters, the mixing fraction of $|\underline{c}d^9 4p\rangle$ in $|\Psi_{\text{fin},1}\rangle$ and $|\underline{c}d^{10}\underline{L}4p\rangle$ in $|\Psi_{\text{fin},2}\rangle$ can be calculated to be $|\sin\theta'|^2\approx0.2$. This indicates that the intensities of features A and C contain about 80% $d^{10}\underline{L}\rangle$ component, while the intensities of features B and D contain about 80% $|d^9\rangle$ component.

B. Electron-doping-induced feature changes

The Ce doping induces a number of interesting spectral changes on the polarized Cu K-edge spectra of $Nd_{2-x}Ce_xCuO_{4-\delta}$ shown in Fig. 2. The feature changes with Ce doping can be summarized as follows: (1) The intensities of features A' and C' increase along with the suppression of the intensities of features B, C, and D; meanwhile feature A located at ~1.9 eV degrades from a prominent peak at $x=0$ to a bump at $x=0.2$. (2) An apparent edge shift in the $\mathbf{E}\perp c$ spectra (see the discussion section, Sec. V D) observed at Ce-doping level $x=0.2$. (3) The peak position of feature B shifts about 0.6 eV upwards at Ce-doping level $x=0.2$. (4) The intensity of feature C decreases relatively less than that of feature D.

With the feature assignment discussed in previous section, observation (1) clearly indicates that Ce doping donates electrons into Cu $3d$ orbitals to form $|d^{10}\rangle$ configuration and simultaneously reduces the $|d^9\rangle$ and $|d^{10}\underline{L}\rangle$ configurations. The intensity reduction of feature A is not as obvious as that of the other features due to the intensity increase of the nearby A' feature. Consistent with this, the low-level doped $Pr_{2-x}Ce_xCuO_4$ ($x\le0.12$) where the A'-feature intensity was smaller,[22] the intensity reduction of feature A was clearly observed. Observation (2), as will be discussed in detail in Sec. V D, can be explained as being primarily due to the intensity increase of the electron-doping-induced new d^{10} feature C'.

With the simple cluster model, observation (3) just means that with Ce doping, the energy separation δE_1 in Eq. (5) increases. This increase can be explained by the decrease of the Δ. Observation (4) (i.e., the slower decrease of the intensity of the feature C than that of the feature D with the increase of x), which was usually left without explanation in the literature, can also be explained by the cluster model. Since $\tan(2\theta)=2V/\Delta$ and $\tan(2\theta')=2V/\Delta'$ with $\Delta'=U_{\underline{c}d}-U_{\underline{c}\underline{L}}-\Delta$, the reduction of Δ will increase θ substantially but decrease θ' only slightly. Thus the ratio of the intensity of feature C to that of feature D, i.e., the I_{rel} in Eq. (6), will increase with the reduction of Δ (or the increase of Ce-doping level x). Since the in-plane Cu $3d_{x^2-y^2}$ states hybridize strongly with the O $2p_{x,y}$ states, Ce doping could shift the $3d_{x^2-y^2}$ (including the d^{10} state) and O $2p_{x,y}$ (containing the $\underline{L}$ state), and thus also the $d^{10}\underline{L}$ state downwards. This shift could reduce the value of the charge-transfer energy Δ in Fig. 1 and increase the value of δE_1 in Eq. (5), which is the energy separation between features A and B (or C and D). This interpretation is consistent with the impurity-state picture proposed by some authors,[10,22,42] i.e., low-level doping of electrons into Cu creates new states (the "impurity states") without significantly effecting the $3d$ band; high-level electron doping joins these new states to the unoccupied $3d$ band and pulls the latter down more. The optical reflectivity measurements of Arima *et al.*[41] on $Pr_{2-x}Ce_xCuO_4$ even suggested that these new states are likely to be composed of hybridized O $2p$ and Cu $3d$ states.

A rough estimate of the reduction of Δ with Ce doping can be made with the use of the model parameters derived earlier, i.e., $U_{\underline{c}d}=6.5$ eV, $U_{\underline{c}\underline{L}}=1.1$ eV, $\Delta=1.35$ eV at $x=0.0$, $V\approx2.7$ eV. If all of the parameters except Δ are assumed unchanged[18] with Ce doping, then the calculated Δ reduction using Eq. (5) is about 0.85 eV for a 0.6-eV increase of δE_1. This result means that Δ is about 0.5 eV at the Ce-doping level $x=0.2$, which is almost the same as that estimated $\Delta=0.4$ eV from some XPS data for $x=0.15$ samples.[18] One should note that an accurate estimate of the Δ dependence of the I_{rel} ($=I_C/I_D$) requires accurate function fitting of the triple peaks C', C, and D and detailed knowledge about the change of the Cu $4p$ DOS with Ce doping. This is due to the fact that the Cu K-edge XAS feature intensities here can be considered as the convolution of the Cu $4p$ partial density states and the spectral lines observed in XPS. Detailed curve fitting results will be reported elsewhere.[43]

C. d^{10} concentration: x correlation

With a clear identification of the A' feature in the $\mathbf{E}\|c$ spectra as the d^{10} feature for both the heavily doped $Nd_{2-x}Ce_xCuO_{4-\delta}$ with $x>0.12$ (in Fig. 2) and the lightly doped $Pr_{2-x}Ce_xCuO_{4-\delta}$ with $x\le0.12$ (in Ref. 22), the d^{10} concentration as a function of the Ce-doping level x in the entire doping range ($0\le x\le0.2$) can be estimated from the intensity of the d^{10} feature A'. The intensity values of the feature A' (located 3.2 eV below feature A) can be estimated approximately by the heights of the peaks (see Sec. V B) in the difference spectra which are obtained by subtracting the $x=0.0$ $\mathbf{E}\|c$ spectrum from the $x\neq0$ $\mathbf{E}\|c$ spectra. Hereafter, the A' feature will be frequently referred to as the Cu^{1+} $4p_\pi$ feature and thus Cu^{1+} only stands for the Cu d^{10} ($N=10$) configuration in the cluster model.

In Fig. 3, the Cu^{1+} $4p_\pi$ intensities are plotted against x for the $Nd_{2-x}Ce_xCuO_{4-\delta}$ single crystals. Note that the data points for $x=0.4$ and $x=0.12$ were generated by scaling the values measured from the data of $Pr_{2-x}Ce_xCuO_{4-\delta}$ crystals in Ref. 22. The scaling factors (≈1) at these two x values were derived from the intensity ratio of the Cu^{1+} $4p_\pi$ intensity of the difference spec-

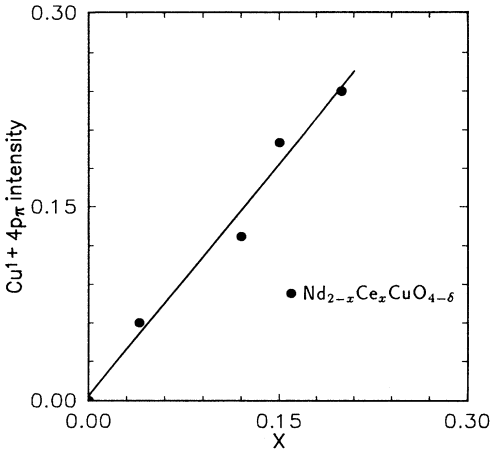

FIG. 3. The peak height of the Cu^{1+} $4p_\pi$ spectral feature obtained from the polarization Cu K-edge difference spectra discussed in the text. All the peak heights have been normalized to the peak height of the Cu^{1+} peak in the difference spectra of powder Cu_2O (see Fig. 4). The data for $x=0.04$ and 0.12 are from the spectra of Ref. 22 and have been discussed in the text.

tra between the $R=$Nd and $R=$Pr powder $R_{2-x}Ce_xCuO_{4-\delta}$ compound series (see Fig. 4). The use of the unpolarized spectra for scaling is justified by the fact that the intensity of feature A' in the powder spectra is dominated by the A' feature in the corresponding $\mathbf{E}\|c$ (see Fig. 5 or Fig. 2 of Ref. 22) spectra. It is clearly seen in Fig. 3 that the intensity of the d^{10} A' feature increases linearly with the increase of the Ce-doping level x. This result unambiguously shows that the Ce-doping continuously injects electrons into Cu $3d$ orbitals to form d^{10}, and the fraction of electron donated by each Ce atom is the same in the entire range of the Ce-doping level $0\leq x\leq 0.2$. To calculate this fractional value, one needs to normalize the Cu^{1+} $4p_\pi$ intensities to the Cu^{1+} $4p_\pi$ intensity of the $\mathbf{E}\|c$ spectra of some Cu^{1+} single-crystal standards. In the absence of polarized Cu K-edge data of such crystals, we will use the unpolarized spectra of powder Cu_2O for determining the Cu^{1+} content later in this paper in the discussion of our $R_{2-x}Ce_xCuO_{4-\delta}$ ($R=$rare earth) results.

V. POLYCRYSTALLINE $R_{2-x}Ce_xCuO_{4-\delta}$

In this section, we study the electron-doping and band-shifting processes in $R_{2-x}Ce_xCuO_{4-\delta}$ compounds with R being all of the rare-earth elements which stabilize the T'-phase structure. Due to the limited availability of single crystals, only the unpolarized Cu K-edge spectra for powder polycrystalline samples will be discussed here. To exclude the effects produced by reduction annealing and to make the analysis systematic, only the spectra for samples annealed in oxygen will be presented. The effects on the Cu K-edge due to the sample reduction process will be briefly discussed in Sec. V D below; more detailed discussion will be presented elsewhere.[43]

A. Feature interpretations

In order to facilitate identification of the spectral features in the unpolarized Cu K-edge spectra for the powder samples, we have plotted in Fig. 5 both the polarized and unpolarized spectra for the $Nd_{1.8}Ce_{0.2}CuO_{4-\delta}$

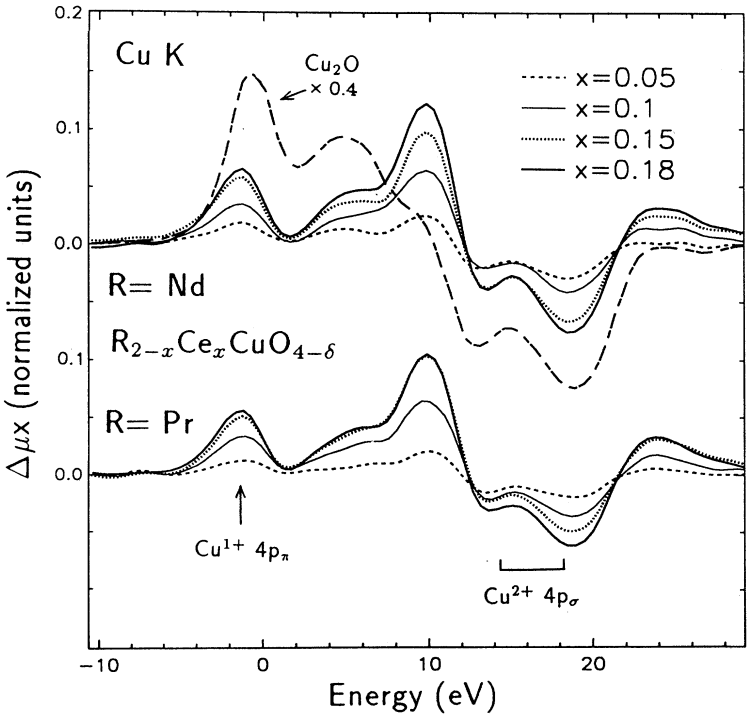

FIG. 4. The difference spectra at the Cu K edge for the polycrystalline $R_{2-x}Ce_xCuO_{4-\delta}$, $R=$Nd and Pr, sample series. The $x=0$ spectra in each series in Fig. 6 were used as Cu^{2+} standards and were subtracted from all of the $x>0$ spectra and Cu_2O spectrum. Note that the intensity of the Cu^{1+} $4p_\pi$ feature in the difference spectra increases with the increase of the Ce-doping level x.

single-crystal and powder samples (all annealed in oxygen). It can be clearly seen that all of the features A', C', and A through D, observed in the polarized spectra, appear in the unpolarized spectrum. Indeed, the unpolarized spectrum of the $x=0.2$ powder sample in Fig. 5 can be well reproduced by the combination of the polarized $\mathbf{E}\perp c$ ($\theta\approx 80°$) and $\mathbf{E}\parallel c$ ($\theta=15°$) spectra using the formula $\sigma(\theta)=\sigma_c\cos^2(\theta)+\sigma_{ab}\sin^2(\theta)$. Here σ_c and σ_{ab} are the absorption cross sections with the polarization vector $\mathbf{E}$ along the c axis ($\theta=0°$) and in the ab plane ($\theta=90°$), respectively, and the value of θ is set at about 63° for the powder spectrum. This procedure justifies the use of the same feature assignments as used in the polarized studies (see Fig. 2).

In view of the above it can be anticipated that the Ce-doping-induced feature changes in the powder K-edge spectra should resemble those feature changes observed in both the $\mathbf{E}\parallel c$ and $\mathbf{E}\perp c$ polarized spectra in Fig. 2. Indeed, it can be seen from Fig. 5 (and Fig. 6) that as x increases from 0.0 to 0.2 in $Nd_{2-x}Ce_xCuO_4$, the intensity of the Cu^{1+} (or d^{10} configuration) features A' and C' increases, concomitant with the decrease of the intensities of the Cu^{2+} (or d^9 and $d^{10}\underline{L}$ configurations) features A through D. These trends are the same as those observed in the polarized spectra (in Fig. 2) as discussed previously.

B. x dependence of Cu^{1+} content

Figure 6 shows the Cu K near-edge spectra for the polycrystalline $R_{2-x}Ce_xCuO_{4-\delta}$ compounds with $0\le x\le 0.18$ and R = Nd, Pr, Sm, Eu, Gd. It can be seen that with Ce doping, x dependence of the spectral features for all of these compounds varies in the same manner as in the R = Nd series. This indicates that the electron-doping effects are almost identical in all of the T'-phase series with different R elements. To see this point more clearly, we will analyze below the quantitative Cu^{1+}-x correlation and the R dependence of the in-plane band shift for all of these series.

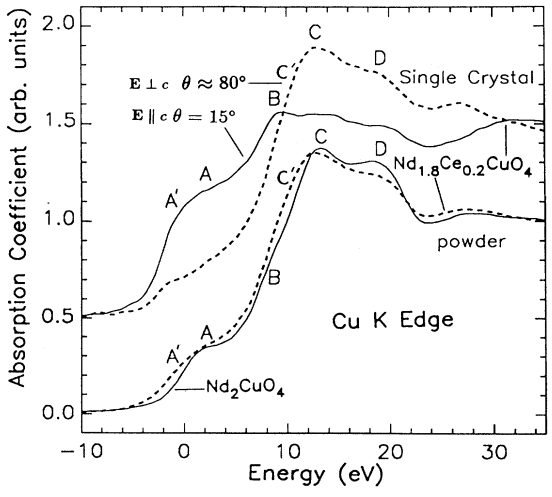

FIG. 5. Polarized Cu K-edge spectra for single-crystal $Nd_{1.8}Ce_{0.2}CuO_{4-\delta}$ and for polycrystalline $Nd_{2-x}Ce_xCuO_{4-\delta}$, $x=0$ and 0.2. θ is the angle between the $\mathbf{E}$ vector and the c axis of the crystal.

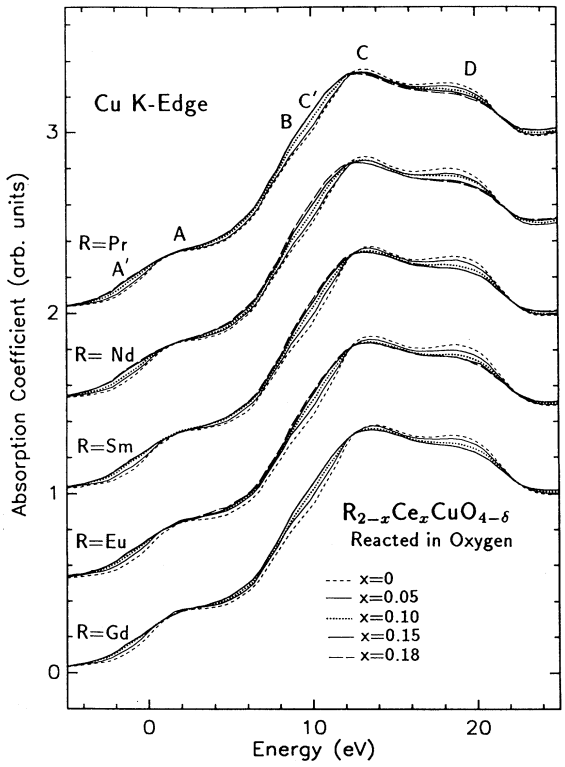

FIG. 6. Cu K-edge spectra for polycrystalline oxygen-annealed $R_{2-x}Ce_xCuO_{4-\delta}$, R = Pr, Nd, Sm, Eu, Gd, and $0<x\le 0.18$.

The quantitative determination of Cu^{1+} content, in copper complexes of a mixed oxidation state, using the intensity of the Cu^{1+} peak of the difference spectra, has been applied previously to various systems.[4,44,45] The study of Hodgson's group[44,45] has shown that the amplitude (~0.49–0.54) of the Cu^{1+} preedge feature intensities, for multitude Cu^{1+} compounds with three or four Cu coordination numbers (CN's), are quite insensitive to the ligand geometry and chemical environment of the Cu. Thus, this amplitude value can be used to estimate the Cu^{1+} component of mixed Cu^{1+}/Cu^{2+} compounds with CN=4 such as $R_{2-x}Ce_xCuO_{4-\delta}$ compounds. We use the intensity of the Cu^{1+} $4p_\pi$ feature of Cu_2O (which has CN=2) for Cu^{1+} estimate because it has almost the same amplitude (~0.54) (Refs. 43 and 44) in its difference spectrum as that for the Cu^{1+} compounds with CN=3 and 4. The error of such an estimate is expected to be about 10%. It should be noted that the Cu K-edge XAS measurements do not directly measure the weight of the various Cu $3d$ configuration. In general, the intensities of the spectral features are influenced by the Cu $4p$ unoccupied density of states (DOS) and $1s\rightarrow 4p$ matrix element, although the relative constancy of the Cu^{1+} preedge feature intensity (with CN=3 or 4) seems to indicate these effects are not large.

The Cu^{1+} content of $R_{2-x}Ce_xCuO_{4-\delta}$ can be estimated from the intensity of the A' [the $4p_\pi(d^{10})$] feature in the difference spectra which were obtained from subtracting the powder spectra of the undoped ($x=0$) sample from those of the Ce-doped (the $x\neq 0$) samples in each series. Figure 4 shows, for example, such difference spectra for the $R=$Nd and Pr series. Also plotted in Fig. 4 is the difference spectrum of the Cu^{1+} standard material Cu_2O, which was obtained by subtracting the Nd_2CuO_4 spectrum. The intensities of the peaks located at ~9.7 eV in the different spectra in Fig. 4 are predominantly C' feature induced and thus also can be used for estimating the Cu^{1+} content. However, since the very nearby B feature (see Fig. 6) variation also contributes to these intensities, we believe that more accurate results can be obtained by using A'-feature intensity than by using the C'-feature intensity. In Fig. 7, we plot the values of the $Cu^{1+}4p_\pi(d^{10})$ intensities (normalized to that of the Cu_2O difference spectrum) against the Ce-doping level x for all of these R series. These normalized Cu^{1+} $4p_\pi$ intensities should yield the $|d^{10}\rangle$ concentration on the Cu sites. The linear relation between the Cu^{1+} intensity and Ce-doping level x, observed previously in the single crystals, is again seen here in the $R=$Nd and Pr polycrystalline series. For $R=$Sm, Eu, and Gd, the dependence of Cu^{1+} on x appears to deviate somewhat from a linear relation, indicating that the electron doping from Ce into Cu $3d$ orbital may become harder as the doping level x becomes larger in these series. The value of the slopes of the fitted straight lines in Fig. 7 is about 0.95 ± 0.05 for all the series except the $R=$Gd series. For the $R=$Gd series, the value is 0.82 ± 0.05.

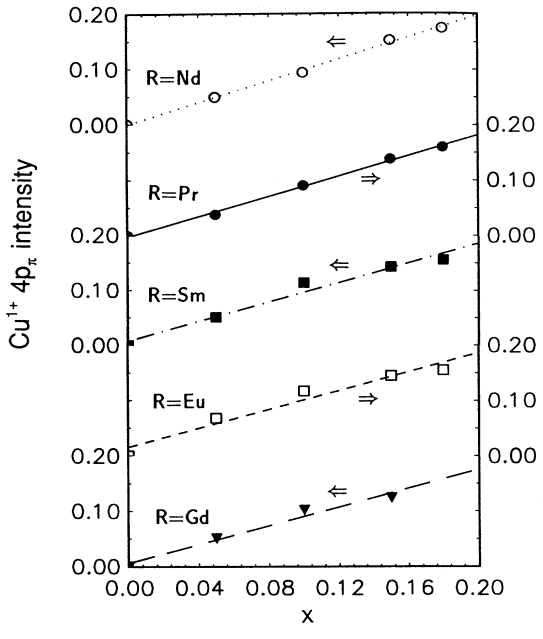

FIG. 7. The peak height of the Cu^{1+} $4p_\pi$ spectral feature in the difference spectra (see Fig. 4 for example) obtained by subtracting the $x=0$ spectra in each $R_{2-x}Ce_xCuO_{4-\delta}$ series of Fig. 6 from the $x\neq 0$ spectra. All the peak heights have been normalized to the peak height of the Cu^{1+} peak in the difference spectra of powder Cu_2O (see Fig. 6). Note the almost linear relation between the Cu^{1+} $4p_\pi$ intensity and the Ce-doping level x.

Thus, we conclude that the average fraction of the electrons doped into Cu $3d$ orbitals from each Ce atom is close to (but slightly smaller than) unity in the $R_{2-x}Ce_xCuO_{4-\delta}$ materials with $R=$Nd, Pr, Sm, and Eu, but shows a 15% decrease for the $R=$Gd series. This conclusion is supported by the proposal of Goodenough *et al.*,[46] i.e., if the Cu-O bond length in the CuO_2 planes of the T' structure is too small, as in the $R=$Gd series, the planes do not readily accept antibonding electrons into the upper $3d_{x^2-y^2}(\sigma^*)$ band.[46] This conclusion is also consistent with the recent result from the transport measurements of $(Nd,Gd,Ce)_2CuO_4$ which indicated the number of charge carriers increases with the substitution of Nd for Gd.[47]

C. *R*-variation effects on Cu *K*-edge spectra

1. *Observations*

Figure 8 shows the Cu K-edge spectra of the powder $R_{2-x}Ce_xCuO_{4-\delta}$ samples with $x=0$ and 0.15. The following effects on the Cu K-edge spectra are observed upon the R-element variation from larger to smaller size, i.e., from Pr→Nd→Sm→Eu→Gd: there is about a $\Delta E=0.48\pm0.05$ eV overall upward edge shift of the spectra, including the whole region of the D feature (but between Eu and Gd an anomalous slight downward shift occurs); the shift is noticeably smaller in the energy region where the intensity is dominated by the $4p_\pi$ features A' and A than in the main edge region (i.e., above 5 eV) where the intensity is dominated by the $4p_\sigma$ features C and D; and the intensity ratio $I_{\rm rel}(=I_C/I_D)$ decreases slowly and continuously, which is clearly seen in the $x=0$ spectra in which the electron-doping-induced C' feature is absent.

Since all of the R elements in the T'-phase materials are trivalent[31] and the Ce-doping level x for the $x=0.15$ spectra in Fig. 8 is the same, these R-variation spectral changes must be attributed to the lattice compression and should be electron-doping independent. This last point is verified by the presence of the same changes in Fig. 8 in the spectra of the undoped R_2CuO_4 compounds. Indeed, the same R-variation-induced spectral changes have been observed in the $R_{2-x}Ce_xCuO_{4-\delta}$ material at all Ce-doping levels (i.e., $0\leq x\leq 0.18$). In Fig. 9, we show the dependence of the edge-energy shift ΔE (measured relative to the edge spectrum of $Pr_2CuO_{4-\delta}$) on the R-element variation in the entire Ce-doping range ($0\leq x\leq 0.18$) of the $R_{2-x}Ce_xCuO_{4-\delta}$ materials. Figure 9 shows that the ΔE versus R curves for different x values are nearly parallel to each other. This indicates that the magnitudes of the edge shifts of the K-edge spectra due to the variation of R from Pr→Nd→Sm→Eu→Gd are basically independent of the Ce-doping level x. Figure 9 also indicates that the edge shift is basically upwards with the decrease of the R-element size but with a slight downward shift seen for R from Eu to Gd.

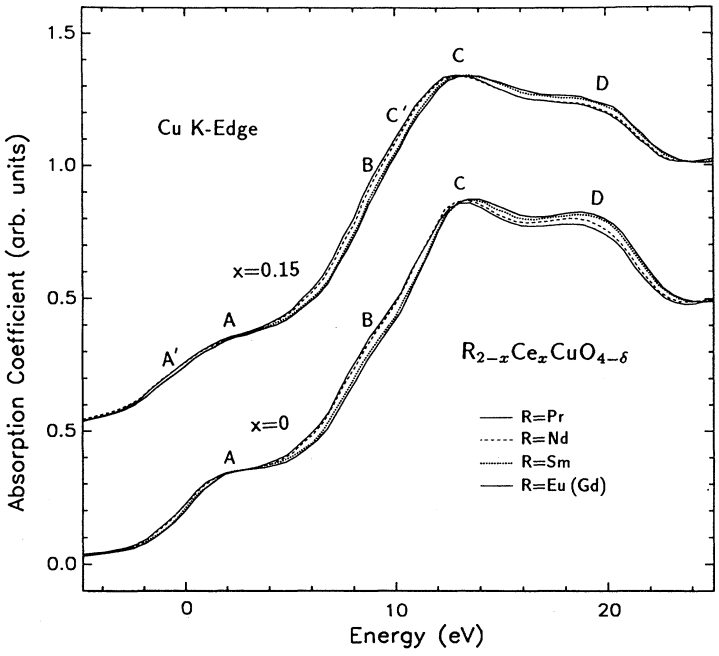

FIG. 8. The Cu K-edge spectra for $R_{2-x}Ce_xCuO_{4-\delta}$ series with $x=0$ and 0.15. Note the almost-rigid shift of the spectra toward higher energy upon R-element variation from larger size at $R=$Pr to smaller size at $R=$Eu (and Gd). The spectra for $R=$Gd are not shown because they are very close to those for $R=$Eu.

2. *Interpretation of the Cu K-edge feature changes*

We now turn a discussion of the origins of the R-variation-induced feature changes of the Cu K edge, particularly the origins of the edge shift. We tentatively interpret this R-element-induced edge shift as due to the shift of the unoccupied in-plane Cu $4p$ states. This interpretation is consistent with the fact that the main-edge region (i.e., the region from post-A feature to post-D feature) shifts almost rigidly with R variation (see Fig. 8). The previously mentioned relatively smaller shift of the spectra (in Fig. 8) in the A'-A feature region than in the B-C'-C-D region can be understood by the fact that the intensity of the powder spectra in the A'-A region is dominated by the contribution from the transition from $1s$ to out-of-plane $4p_\pi$ final states, thus the intensity change due to the shift of the in-plane $4p_\sigma$ states in this region should appear relatively weaker than in the other regions.

Second, this proposal is qualitatively consistent with the ligand field (or crystalline field) theory. Cu in the T' structure has a square planar coordination, i.e., with four oxygen ligands around a central Cu in the CuO_2 plane. As the rare-earth elements R are varying from $R=$Pr towards $R=$Gd, the lattice parameters a and c are decreasing,[30] and thus the four oxygen ligands are moving towards the central Cu ion. According to the ligand field theory,[48,49] the repulsive forces exerted by the ligands due to this compression will raise the energies of the in-plane Cu $4p_\sigma$ antibonding orbitals. In contrast, the out-of-plane $4p_\pi$ orbitals should be less affected and thus the energies are less changed by the lattice compression. The upward shift of the $4p_\sigma$ states would in turn produce an upward shift of the $4p_\sigma$ features C and D and thus an overall shift of the K edge in the main-edge region (i.e., where the $4p_\sigma$ features C'-C-D dominate). On the other hand, the relatively smaller shift of the $4p_\pi$ states will produce a relatively smaller shift in the region where the spectral intensity is dominated by the $4p_\pi$ features A' and A. This is in complete accord with the observations mentioned above.

It should be noted that the change of the ligand field also raises the energies of the Cu $3d$ orbitals upon the compression of the square planar complex. The influence of the a-compression-induced ligand-field change on the in-plane Cu $3d_{x^2-y^2}$ orbital should be much greater than on the other Cu $3d$ orbitals (i.e., $3d_{xy}$, $3d_{xz}$, $3d_{yz}$, and $3d_{z^2}$) and thus the energy of the $d_{x^2-y^2}$ orbital will be

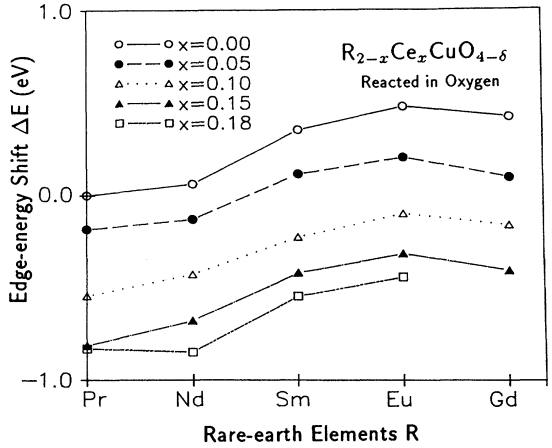

FIG. 9. The dependence of the edge-energy shift ΔE on the rare-earth elements R for $R_{2-x}Ce_xCuO_{4-\delta}$ compounds at different Ce doping levels x. Here the edge-energy shift is measured relative to the edge energy of the $Pr_2CuO_{4-\delta}$ spectrum. Note the similar behavior of the ΔE vs R curves at different Ce-doping levels x.

raised most.[48,49] The observation (mentioned earlier) that I_{rel} decreased with decreasing R size, can also be rationalized by the upward shift of the Cu $3d_{x^2-y^2}$ states (due to lattice compression) in the light of the cluster model. In contrast to the earlier discussion in Sec. IV B, here the upward shift of the Cu $3d_{x^2-y^2}$ states will increase the charge-transfer energy Δ which is the energy gap between the energies of the $3d^{10}\underline{L}$ and $3d^9$ configurations in the cluster model (see Fig. 1). If the other model parameters are assumed unchanged upon the lattice compression, then I_{rel} will decrease with the increase of Δ. However, compared with the Ce-doping induced I_{rel} change (see Fig. 6), I_{rel} decrease caused by R variation is relatively smaller. Our proposal (based on cluster model here) that Δ increases with decreasing R size is also supported by recent optical edge-shift results of Cooper *et al.*[41] which showed a 0.25-eV linear increase of Δ with the decrease of R size from R =Pr to Gd.

D. Discussions

Below we would like to comment on three issues not discussed in detail in the above text.

C' feature versus edge shift. As discussed above, we have attributed the edge shift, caused by R variation, to the upward shift of the unoccupied Cu $4p_\sigma$ band. The shift of the edge upon the R variation (at a fixed electron-doping level x) originates solely from the lattice compression induced ligand-field change. The magnitude of this compression effect can be estimated by noting that for x =0.15 from Eu to Pr one has Δa =0.052 Å leading to a compression shift rate of −9.6 eV/Å. We note that Ce substitution in the $Nd_{2-x}Ce_xCuO_{4-\delta}$ system also entails an a-axis dilatation of Δa =0.008 Å (from x =0.0 to 0.2) and hence the lattice-induced edge shift anticipated would be −0.08 eV. In fact the spectral changes noted in the E⊥c spectra between x =0 and 0.2 would require the much larger shift value of −1.3 eV if interpreted solely in terms of a rigid spectral shift. With this motivation we wish to return to the C' feature versus edge shift discussion deferred from Sec. IV A.

As noted in Sec. IV A, both an appearance of a C' feature and the occurrence of a downward edge shift could introduce similar changes in the $x\neq 0$ E⊥c spectra. The presence of a C' feature analogy to the A' feature is certainly appealing in terms of the model interpretation. Moreover, as noted above, a lattice dilation mechanism (as originally proposed) for an edge shift is not of the proper magnitude to explain the data. There is also additional circumstantial evidence supporting the C' feature origin of the spectral weight increase (with increasing Ce substitution) in the E⊥c spectrum. In the case of the R variation in the (constant x) $R_{2-x}Ce_xCuO_4$ material, for example, where an edge shift is clearly operative, one distinctly sees a concomitant shift in energy of the spectral weight in the C-feature, D-feature, and post-D-feature ranges (see Fig. 8). In contrast the E⊥c $Nd_{2-x}Ce_xCuO_{4-\delta}$ spectra (see Figs. 2 and 6) such concomitant shifts are not seen. Thus there is both motivation and evidence which is in favor of the presence of an electron-doping-induced C' feature and *against* the edge-shift interpretation. Moreover, the C'-feature intensity interpretation is inherently inconsistent with the cluster model which predicts that the d^{10} features should appear in *both* the E⊥c and E∥c spectra with electron doping. Indeed the energy separation between the C' and C features (estimated from Figs. 4 and 6), is about 3.2–3.5 eV, which is almost the same as the energy separation between A' and A features. On the other hand, the missing C' feature in the band-shift interpretation is in conflict with this cluster model prediction. In our opinion, the C'-feature interpretation of the apparent edge shift in the E⊥c spectra in Fig. 2 is more natural and reasonable than the edge shift (or $4p_\sigma$ band shift) interpretation.

In fairness, however, it should be noted that a simultaneously role of a downward edge shift cannot be completely ruled out based on the difference spectral data (Fig. 4) for the present set of materials. The uncertainty arises naturally from the fact that the C' feature has a weak, broad, and unresolved character and is riding on the steeply rising part of the edge. In an attempt to shed light on this issue, difference spectra were calculated using shifted and unshifted x =0 spectra (as in Fig. 4). These shifted difference spectra yield structures in the same energy range as expected from the occurrence of a C' feature. Considering the additional uncertainties introduced by the C and D feature intensity decrease with x, it was found that such difference spectra cannot be used to definitively separate the C' versus edge-shift contributions to the spectra in this range. Definitive resolution of this interesting spectral question will have to await higher signal to noise, higher resolution, and better oriented single-crystal measurements. Perhaps the higher resolution available at the Cu L_1 edge could provide this answer. Toward this end higher surface area crystals or epitaxial films would also be extremely useful, if used in conjunction with multielement detectors (to eliminate Bragg reflection signals).

Role of reductions. Since the reduction of samples in vacuum or inert gas is necessary to stabilize superconductivity we would like to comment on our XAS results on reduced materials. We have carried out an extensive Cu K XAS measurements on the $R_{2-x}Ce_xCuO_{4-\delta}$ samples which were reduced very systematically in helium gas. We found the overall effects of reduction (to be presented elsewhere[43]) on the Cu K edge is negligibly small when compared with the Ce-doping and R-variation-induced effects. Figure 10 shows the effect of reduction on the Cu K edge of the x =0.15 samples as an example. This result is inconsistent with the conclusion of Oyanagi *et al.*[12] who proposed an equivalency of Ce doping and reduction. Further this result is inconsistent with reduction-induced impurities.[43] Our results do favor the direct extension of our basic conclusions on unreduced materials to the reduced materials.

T_c coupling to Cu bands. It is well known that in general, both the Ce doping[1–3,6] and the increase of the size of the R elements[30] in the T' structure $R_{1.85}Ce_{0.15}CuO_{4-\delta}$ materials induce superconductivity and/or enhance T_c (see Fig. 11). The anomalous small depression of T_c between Nd and Pr could be related to the approaching T' structure stability limit.[50] In the

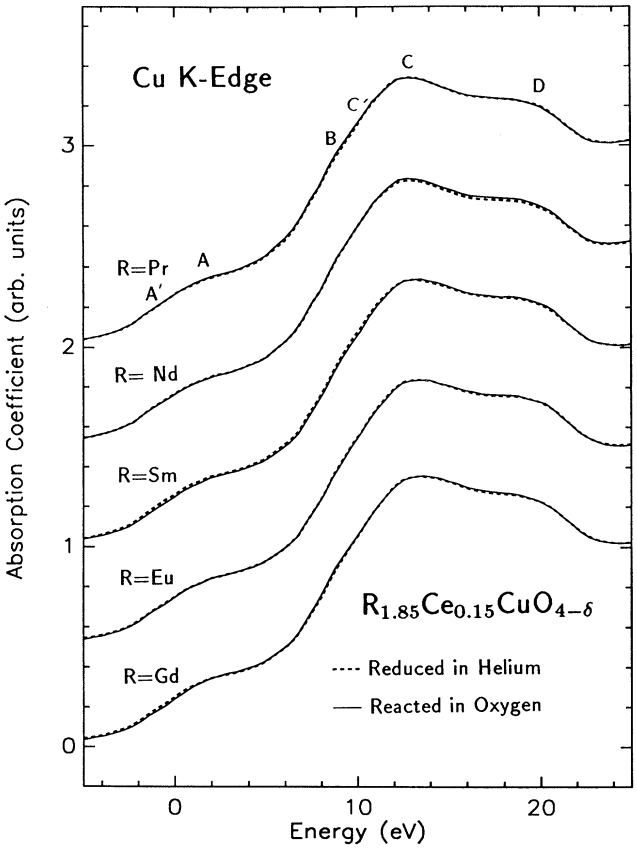

FIG. 10. The Cu K-edge spectra of the polycrystalline $R_{1.85}Ce_{0.15}CuO_{4-\delta}$ compounds comparing the oxygen-annealed samples with the helium-reduced samples. Note that there is almost no change of the spectra due to the reduction of samples.

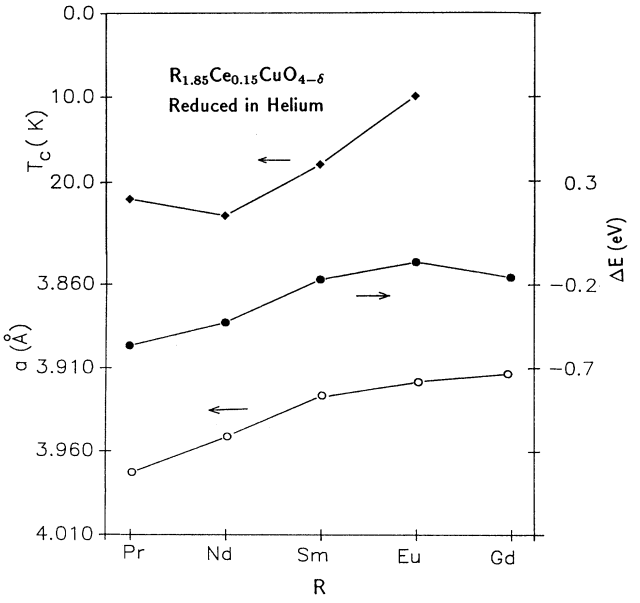

FIG. 11. The rare-earth element dependence of the superconducting transition temperature T_c (solid diamonds), edge-energy shift ΔE (solid circles), and lattice parameter a (open circles) of the helium reduced $R_{1.85}Ce_{0.15}CuO_{4-\delta}$ samples.

present XAS study, we see a clear correlation between the T_c and R size increase caused downward shifts of the Cu K edge (and thus the Cu $4p$ and $3d$ bands shifts, as discussed earlier). Such correlation suggests that it is the downward shifts of the unoccupied Cu bands towards the Fermi energy that are the underlying positive contributing factors in enhancing the superconducting properties (e.g., T_c) in these n-type superconductors. There are, of course, other factors, such as the optimal charge carrier concentration for charge carrier pairing (appearing to be around $x=0.15$), which are critical in determining T_c.

VI. SUMMARY

We have reported systematic polarized and unpolarized Cu K XANES studies on a wide range of T' structure electron-doped high-T_c materials. Our work indicates the continuous Ce-substitution-induced doping of electrons into the Cu $3d$ orbitals over the entire range of substitution (as evidenced by the A'- and C'-d^{10} feature variation in the Cu K-edge spectra). The C'-feature interpretation proposed through the present study appears more acceptable over the edge-shift interpretation in explaining the present E⊥c spectra. The efficiency of the Cu $3d^{10}$ state production per Ce substitute is constant and close to unity for all of the rare-earth hosts, with the exception of the Gd compounds where this efficiency is somewhat reduced. The Ce substitution was also shown to decrease the charge-transfer gap energy Δ.

In addition we have found that a-axis compression (effected by the variation of the trivalent rare-earth elements from Pr to Gd) caused an about 0.5-eV edge shift towards higher energy and the decrease of the relative intensity ratio of the $4p_\sigma$ features C to D. These effects were attributed to the shift of unoccupied Cu $4p$ and $3d$ bands in response to the change of the ligand field. The decrease of T_c with the increase of the size of R elements was correlated to this band shift.

A cluster model description was developed to explain the spectral feature changes induced by electron doping and by the variation of the size of the rare-earth elements. The experimental results support the choice of model parameters with the following values: Cu $1s$-$3d$ Coulomb interaction $U_{cd}\sim 6.5$ eV; Cu $1s$-O $2p$ Coulomb interaction $U_{cL}\sim 1.1$ eV; Cu $3d$-O $2p$ ligand hybridization $V\sim 2.7$ eV; and Cu↔O charge-transfer energy $\Delta\sim 1.3$ eV (at $x=0$) and $\Delta\sim 0.5$ eV (at $x=0.2$).

ACKNOWLEDGMENTS

We thank Dr. Zhengquan Tan for sending us his single-crystal Nd_2CuO_4 data and acknowledge helpful discussion with Dr. John Tranquada. We thank the staff at X-11A beam line of the National Synchrotron Light Source for their assistance in the x-ray absorption measurements. This work was supported by an award from Research Corporation, Sam Houston State University Faculty Research Enhancement Funds, the Robert A. Welch Foundation Grant No. F-1191, and the National Science Foundation Grant No. DMR-9158089.

[1]Y. Tokura, H. Takagi, and S. Uchida, Nature (London) **337**, 344 (1989).

[2]H. Takagi, S. Uchida, and Y. Tokura, Phys. Rev. Lett. **62**, 1197 (1989).

[3]J. T. Markert and M. B. Maple, Solid State Commun. **70**, 145 (1989); J. T. Markert, E. A. Early, T. Bjornholm, S. Ghamaty, B. W. Lee, J. J. Neumeier, R. D. Price, C. L. Seaman, and M. B. Maple, Physica C **158**, 178 (1989).

[4]J. M. Tranquada, S. M. Heald, A. R. Moodenbaugh, G. Liang, and M. Croft, Nature (London) **337**, 720 (1989).

[5]E. E. Alp, S. M. Mini, M. Ramanathan, B. Dabrowski, D. R. Richads, and D. G. Hinks, Phys. Rev. B **40**, 2617 (1989).

[6]G. Liang, J. Chen, M. Croft, K. V. Ramanujachary, M. Greenblatt, and M. Hegde, Phys. Rev. B **40**, 2646 (1989).

[7]Z. Tan, J. I. Budnick, J. L. Peng, and R. N. Shelton, Physica B **163**, 13 (1990).

[8]A. Grassmann, J. Strobel, M. Klauda, J. Schlotterer, and G. Saemann-Ischenko, Europhys. Lett. **9**, 827 (1989).

[9]A. Fujimori, Y. Tokura, H. Eisaki, H. Takagi, S. Uchida, and E. Takayama-Muromachi, Phys. Rev. B **42**, 325 (1990).

[10]T. Suzuki, M. Nagoshi, Y. Fukuda, K. Oh-ishi, Y. Syono, and M. Tachiki, Phys. Rev. B **42**, 325 (1990).

[11]N. Kosugi, Y. Tokura, H. Takagi, and S. Uchida, Phys. Rev. B **41**, 131 (1990).

[12]H. Oyanagi, Y. Yokoyama, H. Yamagachi, Y. Kuwahara, T. Katayama, and Y. Nishihara, Phys. Rev. B **42**, 10 136 (1990).

[13]E. Lederman, L. Wu, M. L. Denbore, D. A. van Aken, W. F. Muller, and S. Horn, Phys. Rev. B **44**, 2320 (1991).

[14]A. Krol, C. S. Lin, Z. H. Ming, C. J. Sher, Y. H. Kao, C. L. Lin, S. L. Qiu, J. Chen, J. M. Tranquada, M. Strongin, G. S. Smith, Y. K. Tao, R. L. Meng, P. H. Hor, C. W. Chu, G. Gao, and J. E. Crow, Phys. Rev. B **42**, 4763 (1990).

[15]C. F. J. Flipse, G. Van der Laan, A. L. Johnson, and K. Kadowaki, Phys. Rev. B **42**, 1997 (1990).

[16]S. Uji, M. Shimoda, and H. Aoki, Jpn. J. Appl. Phys. **28**, L804 (1989).

[17]M. K. Rajumon, D. D. Sarma, R. Vijayaraghavan, and C. N. R. Rao, Solid State Commun. **70**, 875 (1989).

[18]H. Ishii, T. Koshizawa, H. Kataura, T. Hanyu, H. Takai, K. Mizoguchi, K. Kume, I. Shiozaki, and S. Yamaguchi, Jpn. J. Appl. Phys. **28**, L1952 (1989).

[19]Y. Hwu, M. Marsi, A. Terrasi, D. Rioux, Y. Chang, J. T. Mckinley, M. Onellion, G. Margaritondo, M. Capozi, C. Quaresima, A. Campo, C. Ottaviani, P. Perfettic, N. G. Stoffel, and E. Wang, Phys. Rev. B **43**, 3678 (1991).

[20]N. Nücker, P. Adelmann, M. Alexander, H. Romberg, S. Nakai, J. Fink, H. Rietschel, G. Roth, H. Schmidt, and H. Spille, Z. Phys. B **75**, 421 (1989).

[21]M. Alexander, H. Romberg, N. Nücker, P. Adelmann, J. Fink, J. T. Markert, M. B. Maple, S. Uchida, H. Takagi, Y. Tokura, A. C. W. P. James, and D. W. Murphy, Phys. Rev. B **43**, 333 (1991).

[22]Z. Tan, J. I. Budnick, C. E. Bouldin, J. C. Woicik, S-. W. Cheong, A. S. Cooper, G. P. Espinosa, and Z. Fisk, Phys. Rev. B **42**, 1037 (1990).

[23]H. Tolentino, M. Medarde, A. Fontaine, F. Baudelet, E. Dartyge, D. Guay, and G. Tourillon, Phys. Rev. B **5**, 8091 (1992).

[24]T. C. Huang, E. Moran, A. I. Nazzal, and J. B. Torrance, Physica C **158**, 148 (1989).

[25]R. Saez Puche, M. Norton, and W. S. Claunsinger, Mater. Res. Bull. **17**, 1523 (1982).

[26]S-. W. Cheong, J. D. Thompson, and Z. Fisk, Physica C **158**, 109 (1989).

[27]P. H. Hor, R. L. Meng, Y. Q. Wang, L. Gao, Z. J. Huang, J. Bechtold, K. Forster, and C. W. Chu, Phys. Rev. Lett. **58**, 1891 (1987).

[28]Z. Fisk, J. D. Thompson, E. Zirngiebl, J. L. Smith, and S-. W. Cheong, Solid State Commun. **63**, 515 (1987).

[29]J. M. Tarascon, W. R. McKinnon, L. H. Greene, G. H. Hull, and E. M. Vogel, Phys. Rev. B **36**, 226 (1987).

[30]J. T. Markert, J. Beille, J. J. Neumeier, E. A. Early, C. L. Seaman, T. Moran, and M. B. Maple, Phys. Rev. Lett. **64**, 80 (1990).

[31]Z. Tan, S. M. Heald, S-. W. Cheong, A. S. Cooper, and J. I. Budnick, Phys. Rev. B **45**, 2593 (1992); M. Tovar, D. Rao, J. Barnett, S. B. Oseroff, J. D. Thompson, S-. W. Cheong, Z. Fisk, D. C. Vier, and S. Schulz, *ibid.* **39**, 2661 (1989).

[32]V. J. Emery, Phys. Rev. Lett. **58**, 2794 (1987); V. J. Emery and G. Reiter, Phys. Rev. B **38**, 4547 (1988); C. M. Varma, S. Schmitt-Rink, and E. Abrahamas, Solid State Commun. **62**, 681 (1987).

[33]A. K. McMahan, R. M. Martin, and S. Satpathy, Phys. Rev. B **38**, 6650 (1989).

[34]M. S. Hybertsen, M. Schlüter, and N. E. Christenser, Phys. Rev. B **39**, 9028 (1989).

[35]Z. X. Shen, S. W. Allen, J. J. Yeh, J. S. Kang, W. Ellis, W. Space, I. Lindau, M. B. Maple, Y. D. Dalichaouch, M. S. Torikachvili, J. Z. Sun, and T. H. Geballe, Phys. Rev. B **36**, 8414 (1987), and references therein.

[36]For example, see D. D. Sarma and S. G. Ovchinnikov, Phys. Rev. B **42**, 6817 (1990), and references therein.

[37]J. Zaanen, G. A. Sawatzky, and J. W. Allen, Phys. Rev. Lett. **55**, 418 (1985).

[38]C. T. Chen, F. Sette, Y. Ma, M. S. Hybertsen, E. B. Stechel, W. M. C. Schluter, S-W. Cheong, A. S. Cooper, L. W. Rupp, Jr., B. Batlogg, Y. L. Soo, Z. H. Ming, A. Krol, and Y. H. Kao, Phys. Rev. Lett. **66**, 104 (1991); L. H. Tjeng, C. T. Chen, and S-W. Cheong, Phys. Rev. B **45**, 8205 (1992).

[39]R. A. Bair and W. A. Goddard III, Phys. Rev. B **22**, 2767 (1980).

[40]N. Kusugi, T. Yokoyama, K. Asakura, and H. Kuroda, Chem. Phys. **91**, 249 (1984).

[41]S. L. Cooper, G. A. Thomas, A. J. Millis, P. E. Sulewski, J. Orensrein, D. H. Rapkine, S-W. Cheong, and P. L. Trevor, Phys. Rev. B **42**, 10 785 (1990); T. Arima, K. Kikuchi, M. Kasuya, S. Koshihara, Y. Tokura, T. Ido, and S. Uchida, *ibid.* **44**, 917 (1991).

[42]J. W. Allen, C. G. Olson, M. B. Maple, J. S. Kang, L. Z. Liu, J.-H. Park, R. O. Anderson, W. P. Ellis, J. T. Markert, Y. Dalichaouch, and R. Liu, Phys. Rev. Lett. **64**, 595 (1990).

[43]G. Liang *et al.* (unpublished).

[44]Lung-Shan Kau, Darlene J. Spira-Solomon, James E. Penner-Hahn, Keith O. Hodgson, and Edward I. Solomon, J. Am. Chem. Soc. **109**, 6433 (1987).

[45]J. E. Penner-Hahn, B. Hedman, K. O. Hodgson, D. J. Spira, and E. I. Solomon, Biochem. Biophys. Res. Commun. **119**, 567 (1984).

[46]J. B. Goodenough, Supercond. Sci. Technol. **3**, 26 (1990); J. B. Goodenough and A. Manthiram, J. Solid State Chem. **88**, 115 (1990).

[47]C. Lin, G. Lu, and Y. F. Zhang, Physica C **194**, 66 (1992).

[48]J. J. Lagowski, *Modern Inorganic Chemistry* (Marcel Dekker, New York, 1973), p. 699; G. N. Brown, *A New Guide to Modern Valence Theory* (Wiley, New York, 1967).

[49]B. N. Figgis, *Introduction to Ligand Fields* (Wiley, New York, 1966).

[50]E. T. Heyen, R. Liu, M. Cardona, S. Piñol, R. J. Melville, D. McK. Paul, E. Morán, and M. A. Alario-Franco, Phys. Rev. B **43**, 2857 (1991).